Article

On MoS TFT Design Consideration for NO Gas Sensor

Healin Im, AbdulAziz AlMutairi, Sehwan Kim, Mayuri Sritharan, Sunkook Kim, and Youngki Yoon

ACS Sens., **Just Accepted Manuscript** • DOI: 10.1021/acssensors.9b01307 • Publication Date (Web): 16 Oct 2019

On MoS_2 TFT Design Consideration for NO_2 Gas Sensor

Healin Im[1], AbdulAziz AlMutairi[2], Sehwan Kim[1], Mayuri Sritharan[2], Sunkook Kim [1,*] and Youngki Yoon[2,*]

[1] School of Advanced Materials Science & Engineering, Sungkyunkwan University, Suwon, 440-745, Republic of Korea; seonkuk@skku.edu.
[2] Department of Electrical and Computer Engineering & Waterloo Institute for Nanotechnology (WIN), University of Waterloo, Waterloo, ON, N2L 3G1, Canada; youngki.yoon@uwaterloo.ca.

Keywords: Transition metal dichalcogenides, field-effect transistors, passivation, chemical sensor, NO_2

Abstract

MoS_2 thin-film transistors (TFTs) are fabricated and simulated to explore NO_2 gas sensing mechanism depending on different device structures. In particular, the role of Al_2O_3 passivation layer on the MoS_2 channel has been investigated. In the case of non-passivated MoS_2 TFTs, increase of OFF current is observed with NO_2 gas, which has been modeled with the modulation of the effective Schottky barrier height for holes, due to the generation of in-gap states near the valence band as NO_2 gases interact with the MoS_2 channel. The non-passivated MoS_2 TFTs are simulated based on non-equilibrium Green's function (NEGF) method, and the simulation results do confirm this sensing mechanism. On the other hand, MoS_2 TFTs with the Al_2O_3 passivation layer has been modeled with a pseudo-double gate structure as NO_2 gases on the capping layer can act like the secondary gate inducing the positive charge state. Our quantum transport simulation shows that significant threshold voltage shift can be achieved with NO_2 gas, which matches the experimental observation, thereby exhibiting completely different sensing mechanism of the passivated device from the non-passivated counterpart. In addition, we also discuss competing device parameters for the passivated MoS_2 TFTs by varying the main and the secondary gate dielectric, suggesting co-optimization to realize high sensitivity and low power consumption simultaneously.

A gas sensor is an essential device for various applications, such as environmental and agricultural monitoring, process control, and diagnostics. Materials for gas sensors require high surface-to-volume ratio, great performance at low operating power, and excellent sensitivity and kinetics[1]. MoS_2, which is a well-known two-dimensional (2-D) layered material, exhibits great potential for gas sensors due to their outstanding properties — ultra-high surface-to-volume ratio[2,3], effective sensitivity to gases[4,5], low power comsumption[6], low operating temperature[7], and the capability of surface functionality[8,9]. Recent studies have reported the functionalization of MoS_2 surface with metal[9,10], metal oxide[11], and nanoparticles[12–16], and the variation in MoS_2 morphology[17–19] to achieve high gas sensitivity with MoS_2 thin-film transistors (TFTs). For examples, MoS_2/SnO_2 nanohybrid sensors can detect NO_2 gas concentration ranging from 0.5 ppm to 10 ppm based on change in conductance[12]. Also, Pd quantum-dots-modified MoS_2 can enhance its responsivity to NO_2 gas 50 times higher than pristine MoS_2 by modifying the material's surface[14]. In addition, vertically standing MoS_2 devices were suggested for highly sensitive NO_2 gas sensors whose detection limit is 0.1 ppm[19]. These approaches mainly focused on the increase of the surface-to-volume ratio to improve sensitivity; whereas other strategies have also been demonstrated for the same purpose, for example, by using a high temperature treatment to create rapid desorption of gases on the channel surface[20] or a light treatment to heal the surface of MoS_2[21,22].

To develop highly sensitive gas sensors, it is necessary to understand gas sensing mechanism clearly, which has been briefly discussed in some of previous studies. It was

reported that the resistance and conductance of 2D materials can be changed when they interact with gas molecules due to the charge transfer between the two[20,21]. Other studies also showed that NO_2 gas can generate sub-gap states, leading to significant change in effective bandgap and increase in leakage current[22,23]. It should be noted that previous studies mainly focused on the modification of material properties without considering the optimization of device structure. However, the sensitivity of gas sensors strongly depends on not only material properties but also proper design of sensor structure, so it is equally important to consider both material properties and device parameter optimization through systematic studies, which is currently missing from the field.

In this paper, we fabricate and model two different MoS_2 TFT gas sensors with and without passivation layer on the surface of MoS_2 channel to investigate different operating mechanisms based on the dissimilar device structure. Current-voltage characteristics obtained from each type of gas sensor under NO_2 gas flow exhibit their unique sensing behaviors. Each type of sensor is modelled and simulated to explain the experimental observations. Modulation of effective Schottky barrier (SB) height is adopted to model non-passivated MoS_2 TFTs[23], whereas pseudo-double gate device simulation[24] is used for passivated MoS_2 gas sensors. Our simulations reveal that NO_2 gas can vary OFF-state leakage current of the device when MoS_2 is exposed, while the gas molecules can act as a secondary gate when sitting on the passivation layer. Furthermore, structural optimization is also discussed based on simulations by varying device parameters such as oxide thickness, which makes it possible to achieve higher sensitivity.

Materials and Methods

Device Fabrication

In the case of non-passivated MoS_2 TFTs, a highly-doped Si/SiO_2 wafer was immersed into buffered oxide etch (BOE) for 10 min to reduce SiO_2. A 40-nm thick high-*k* Al_2O_3 thin film was deposited on the substrate for a gate insulator using atomic layer deposition (ALD). Multilayer MoS_2 was transferred onto Al_2O_3 layer from bulk MoS_2. As-transfer MoS_2 is rinsed in acetone for 1 hour and in isopropyl alcohol (IPA) for 10 min, in order. Then, 10-nm thick Ti and 40-nm thick Au were deposited and patterned using photoresist (PR) and lithography. Before electrical measurement, the transistor was annealed at 200℃ for 2 hours under Ar ambient so that the contact resistances between electrodes and MoS_2 can be reduced. In the case of passivated MoS_2 TFTs, as-fabricated non-passivated MoS_2 TFTs were passivated by Al_2O_3. As-grown Al_2O_3 passivation layer was formed about 20 nm-thick and then contact regions on the electrodes were pattered by PR.

Sensor Measurement

Electrical performance and gas-sensing characteristics of MoS_2 TFTs were monitored using a semiconductor analyzer (Keithley Co., SCS 4200). All the electrical measurements and gas-sensing characterizations of devices were conducted in a closed vacuum chamber at room temperature. NO_2 gas was injected towards the MoS_2 channel directly with a sprayer so that we can observe how electrical properties of MoS_2 TFTs will be changed with NO_2

gas depending on their structures. The desired concentration and flux of NO_2 gas were obtained from mass flow controllers (MFCs) by mixing N_2 diluted 2000 ppm NO_2 gas and 99.999 % N_2 gas. The NO_2 gas flow is controlled by adjusting the ratio of NO_2 gas to N_2 gas while the total gas flow is fixed at 100 sccm. The flow of NO_2 gas is adjusted from 0 sccm to 0.2 sccm in the flow intervals of 0.05 sccm so that the concentration of NO_2 gas can be controlled from 0 ppm and 2000 ppm in the concentration intervals of 500 ppm.

Model and Simulation

Current-voltage characteristics of both types of MoS_2 sensors are calculated based on the non-equilibrium Green's function (NEGF) ballistic quantum transport simulation using the effective mass approximation, self-consistently with the Poisson's equation. Schottky contacts is used at the source-channel and the channel-drain junctions with the Schottky barrier height (Φ_{Bn}) of 0.1 eV for electrons[25]. For a nominal device, we use 0.65 nm-thick, 20 nm-long channel with equivalent oxide thickness (EOT) of the bottom gate oxide of 17.3 nm, which matches the experimental value used. Although we have used much a thinner and shorter channel compared to that of the actual devices to save simulation time, it will not change the underlying physics investigated in this study, thereby making our qualitative conclusion unaffected. Note that width information is implicit in the NEGF simulation; hence, the calculated current value is provided in ampere per unit width. A power supply voltage, V_{DD} = 1 V was used with the source grounded. To represent the non-passivated device, air is assumed on top of the channel with a floating boundary condition. In this case, NO_2 gas molecules introduce in-gap states to the multilayer MoS_2,

which can be interpreted as the modulation of effective Schottky barrier height for holes (Φ_{Bp}) [22,23]. In this study, we have used Φ_{Bp} of 1.13–1.23 eV to reproduce the data from experiment. On the other hand, for the passivated MoS_2 TFTs, Al_2O_3 is used also for the top passivation layer (EOT_{TOP} = 4.3 nm for a nominal device). Due to the passivation layer, NO_2 does not have a direct impact on the band structure of the channel MoS_2; instead, the charge transfer occurs between the NO_2 gas and the top passivation layer, resulting in the positive charge state at the surface of Al_2O_3[24,26]. We model this pseudo-double gate structure by introducing the positive charge density (N) on the passivation layer for the secondary gate effect caused by the NO_2 gas.

Design Optimization

In this work, the optimized sensor design is proposed by engineering two competing parameters − the top and bottom EOTs of passivated MoS_2 TFTs by means of simulation. Moreover, passivated MoS_2 TFTs with different thicknesses of top Al_2O_3 layer (20 nm and 5 nm) are fabricated and their sensing performance such as V_{TH} shift and sensitivity is compared by experiment. To facilitate a fair and direct comparison among different sensor structures, sensitivity under NO_2 gas is defined with I_{gas}/I_0. For the response/recovery characteristics, the target NO_2 concentrations of 100, 200, 300, 400, and 500 ppm are achieved by controlling the NO_2 flow from 0.1 to 0.5 sccm at the constant total flow of 1000 sccm.

Results and Discussions

Figures 1a and b illustrate the structures of non-passivated and passivated MoS_2 TFTs for NO_2 gas sensors, respectively. Depending on the structure of TFTs, their responses to NO_2 can be significantly different. In order to compare two different devices with regard to the response to NO_2 gas, we have chosen devices showing similar electrical properties of pristine MoS_2 TFTs as I_{ON}/I_{OFF} of ~$10^5$with a surface area of ~60 μm^2. Figure 1c shows I_{DS}–V_{GS} curves of non-passivated MoS_2 TFTs with the flow of NO_2 gas at V_{DS} = 1 V. (The width, length and thickness of the channel are 7.26 μm, 8.39 μm and ~40 nm, respectively.) There is a gradual increase in I_{OFF} with the flow of NO_2 gas, while I_{ON} and V_{TH} remain almost unaffected. At V_{GS} = -3 V, as flow of NO_2 gas increases from 0 sccm to 0.2 sccm, I_{OFF} increases from 39.48 pA to 160.86 pA. This response to NO_2 gas, showing a trend of proportional increase of I_{OFF} with NO_2 gas, is a great accordance with previous studies[23]. On the other hand, the passivated MoS_2 TFT with the thickness of ~6.3 μm, the length of 10.14 μm and the thickness of ~30 nm exhibits a negative shift of V_{TH} with a negligible change in I_{OFF} with the flow of NO_2 gas (see Figure 1d). As the flow of NO_2 gas increases from 0 sccm to 0.2 sccm, V_{TH} changes from -0.83 V to -1.05 V towards the negative V_{GS}.

Figures 2a and b show variations in I_{OFF} (at V_{GS} = -3 V) and ΔV_{TH} (obtained from $\sqrt{I_{DS}}$ -V_{GS} curves) depending on the NO_2 flow. As clearly seen from Figure 2a, I_{OFF} of the non-passivated MoS_2 TFT exhibits a linear response to the NO_2 flow while that of the passivated MoS_2 TFT shows no changes. On the other hand, Figure 2b shows significant negative V_{TH} shift for the passivated TFT with increase in NO_2 flow, which is not the case

of the non-passivated MoS_2 TFT. The distinct characteristics of two devices are attributed to different sensing mechanisms. If NO_2 gas molecules are attached to the surface of MoS_2 channel in the non-passivated sensors, in-gap states are created close to the valence band of MoS_2 as shown in Figure 2c[22]. This can facilitate tunneling as the effective Schottky barrier for holes is lowered, which is modeled by the effective Φ_{Bp} modulation to capture the OFF-state leakage current affected[23]. In case of the passivated MoS_2 TFT, negative ΔV_{TH} can be modeled with a secondary gate through the top gate dielectric[24]. If NO_2 gas molecules are located on the surface of Al_2O_3, they can take electrons[26] and make the passivation layer a positive-charge state. Consequently, the potential barrier of the channel can be lowered as shown in Figure 2d, resulting in the increase of current and the negative V_{TH} shift.

Next, using the models explained above, we have performed numerical simulations. Figure 3a shows the simulated I_{DS}–V_{GS} curves of the non-passivated MoS_2 device with three different effective Φ_{Bp} of 1.13, 1.18, and 1.23 eV. Our simulation results show that I_{OFF} increases as Φ_{Bp} is reduced, which is analogous with experimental observations with the increased gas flow. This indicates that the operating mechanism of non-passivated MoS_2 TFTs can be explained by the reduction of effective Φ_{Bp} as more NO_2 gas molecules are attached to the MoS_2 channel. Blue asterisks in Figure 3b shows I_{gas}/I_0 as a function of Φ_{Bp} achieved from simulation at V_{GS} = -3 V, where I_0 is the reference drain current for the pristine MoS_2 TFT (Φ_{Bp} = 1.23 eV) and I_{gas} is the current with NO_2 gas (Φ_{Bp} < 1.23 eV). Based on the simulation data, we have modeled the relation between I_{gas}/I_0 and Φ_{Bp}, leading to

$$\log_{10}\left(\frac{I_{gas}}{I_0}\right) = p_1 \Phi_{\mathrm{Bp}} + p_2,$$

where p_1 and p_2 are -13.50 eV^{-1} and 16.56, respectively. The dotted line in Figure 3b represents our model. Next, experimental data for 0 – 0.2 sccm NO_2 gas are also shown in Figure 3b along with the model to derive the relation between the NO_2 gas flow (F) and Φ_{Bp}. The formula is given by

$$\Phi_{\mathrm{Bp}} = p_3 F^2 + p_4 F + p_5,$$

where $p_3 = 1.051$ eV/sccm^2, $p_4 = -0.431$ eV/sccm, and $p_5 = 1.227$ eV. The relation between the two is shown in Figure 3c, which represents that effective Φ_{Bp} reduces linearly with the NO_2 gas flow of 0 – 0.1 sccm but the effective Φ_{Bp} modulation caused by the in-gap state starts to saturate beyond that point.

Similarly, Figure 3d shows the simulated I_{DS}–V_{GS} curves of the passivated MoS_2 TFT with three different conditions: positive charge density (N) of 0, 2×10^{23}, and 4×10^{23} m^{-3}. Our simulation results show that more negative V_{TH} is achieved as N increases. Consequently, ΔV_{TH} due to the secondary gate effect, with respect to the case with no gas condition, becomes negative. Blue asterisks in Figure 3e shows ΔV_{TH} as a function of N, which can be described by

$$\Delta V_{\mathrm{TH}} = q_1 N^2 + q_2 N + q_3,$$

where $q_1 = 5.3229 \times 10^{-49}$ V · m^6, $q_2 = -8.8428 \times 10^{-25}$ V · m^3, and $q_3 = 0.069907$ V. To find the relation between N and NO_2 gas flow (F) giving the same threshold voltage shift, 0 – 0.2 sccm NO_2 gas from experiments (red open squares) are also shown in Figure

3e along with the model (dotted line), resulting in the following relation:

$$N = q_4 F + q_5,$$

where $q_4 = 1.4727 \times 10^{24}$ $m^{-3}sccm^{-1}$ and $q_5 = 1.6203 \times 10^{23}$ m^{-3}. As shown in Figure 3f, N exhibits a linear relation to the gas flow (F) for the entire range considered in this study (0 to 0.2 sccm).

So far, we have investigated different operational mechanisms of non-passivated and passivated MoS_2 TFTs. Next, we will further extend our discussion for sensitivity improvement through design optimization. For non-passivated MoS_2 TFTs, NO_2 gas directly interacts with the MoS_2 channel, so there exists less room for optimization. However, for passivated MoS_2 TFTs, we can engineer two competing parameters: namely, the main bottom gate and the secondary top gate, by carefully tuning top and bottom EOTs. Therefore, we will focus on the optimization of the passivated MoS_2 TFTs below. It is expected that ΔV_{TH} of the passivated MoS_2 TFTs can be more sensitive if thinner EOT_{TOP} is used. Figure 4b exhibits how ΔV_{TH} varies with different EOT_{TOP} for a fixed EOT_{BOT} (17.3 nm) and $N = 3 \times 10^{23}$ m^{-3}. It shows that ΔV_{TH} can be improved from -0.15 V to -0.37 V by changing EOT_{TOP} from 4.3 nm to 1.3 nm. On the other hand, EOT_{BOT} can provide another design freedom to achieve higher sensitivity. Figure 4c shows ΔV_{TH} as a function of EOT_{BOT} with EOT_{TOP} = 1.3 nm for the same gas flow assumed. ΔV_{TH} can be significantly larger by 3.8 times if EOT_{BOT} is changed from 7.3 nm to 27.3 nm. However, at the same time, subthreshold swing (SS) is significantly increased with the same change in EOT_{BOT} (with a fixed EOT_{TOP}) as it can be seen in Figure 4d. It should be noted that

devices with smaller SS is desirable for lower leakage current and less power consumption, which could be important particularly for mobile device applications. The observed trade-off between sensitivity and SS can be explained by the channel potential modulation through the device's main (bottom) gate. Thinner EOT_{BOT} results in better gate control, which can lower SS; however, such a strong control screens the secondary gate effect induced by the NO_2 gas, resulting in lower sensitivity, and vice versa. On the other hand, SS will be less susceptible to EOT_{TOP} as long as EOT_{BOT} will not be changed, as NO_2 gas on the top passivation layer provides only the secondary effect on the switching characteristics. Therefore, it is suggested that sensitivity and fundamental device performance should be considered simultaneously in optimizing parameters of the passivated TFT structure.

As suggested by the numerical simulation, we have also fabricated a passivated MoS_2 TFT with a thinner (5 nm) passivation layer to improve the sensor performance. With 5 nm-thick Al_2O_3, the V_{TH} shift becomes -0.52 V (Figure 5a) and the resulting sensitivity can be ~ 18 (Figure 5b) under 500 ppm of NO_2 gas, which is huge improvement as compared to the sensor with a thicker (20 nm) passivation layer (see Figures 5a and 5b).

Next, time-resolved NO_2 sensing behaviors have been investigated for two different types of MoS_2 TFTs. Figures 6a and 6b present time-resolved current responses of the non-passivated and the passivated MoS_2 TFT with 5 nm-thick Al_2O_3 with different NO_2 gas concentration. After NO_2 gas was injected for 10 min (color lines in Figures 6a and 6b; not scaled) to stabilize the chamber condition, drain currents were measured in real-time. The

non-passivated MoS_2 TFT shows the higher I_{OFF} with increasing NO_2 concentration; however, the current increase is insufficient, and I_{OFF} after NO_2 exposure is gradually degraded over time as shown in Figure 6a. In contrast, the passivated MoS_2 TFT with 5 nm-thick top oxide layer exhibits much more distinguishable current depending on NO_2 concentration, and their signals are cleaner with no noticeable decline in the current level over time (Figure 6b).

Finally, time-resolved ON-OFF switching responses at a NO_2 gas concentration of 500 ppm have been examined. In the ON state, currents were measured in real-time 10 min after NO_2 gas was injected (color lines in Figures 6c and 6d; not scaled). In the OFF state, each device was first recovered for 1 min at V_{GS} = 30 V, which is opposed to the measurement bias, while injecting only N_2 gas (gray lines in Figures 6c and 6d; not scaled), and then current has been measured at the same V_{GS} as in the ON state[23,27]. As shown in Figure 6c, the non-passivated MoS_2 TFT shows relatively poor ON-OFF switching characteristics, and the signal is unstable over time. On the contrary, the passivated MoS_2 TFT with 5-nm top oxide layer shows superior ON-OFF switching responses with stable and clean signals (Figure 6d). Our results indicate that the passivated MoS_2 TFTs with a thin top oxide have great potential for gate-refreshable, high-performance NO_2 gas sensors.

Conclusions

We have investigated structure-dependent NO_2 gas sensing mechanism of MoS_2 TFTs based on both experiment and theory. Fabricated non-passivated MoS_2 TFTs showed that

OFF current increases as the sensor is exposed to more NO_2 gases. We have modeled the sensing mechanism of the non-passivated MoS_2 TFT with the in-gap states induced by NO_2 gas on the MoS_2 surface and the modulation of the effective Schottky barrier height for holes. Our numerical device simulation results are in good agreement with the experiment, thereby confirming the validity of our model for the non-passivated MoS_2 gas sensors. On the other hand, fabricated passivated MoS_2 TFTs exhibit negative V_{TH} shift as the flow of NO_2 gas increases. We have modeled the sensing mechanism by introducing a secondary gate with positive charges on the capping dielectric surface. Our simulation on the pseudo-double gate MoS_2 TFT showed the same negative V_{TH} shift as experiment, indicating that the NO_2 sensing mechanism of the passivated structure is completely different from that of the non-passivated MoS_2 TFT. Furthermore, we have also discussed the design strategy to optimize sensitivity and power consumption simultaneously by careful investigation of the main and the secondary gate dielectric of the passivated MoS_2 TFT. Lastly, as suggested by the numerical simulation results, we have fabricated a passivated MoS_2 TFT with a thinner top passivation layer to further improve the sensor performance, which exhibited significant enhancement not only in V_{TH} shift and sensitivity but also in response/recovery behaviors through design optimization.

Acknowledgments

This research was supported in part by the National Research Foundation of Korea (Grant NRF-2018R1A2B2003558 and 2015R1A5A1037548). This work was supported in part by NSERC Discovery under Grant RGPIN-05920-2014. Computing resources were provided by Calcul Quebec through Compute Canada. M. Sritharan acknowledges the financial

support from NSERC USRA.

Author Contributions

H. Im and A. AlMutairi equally contributed to this work.

References

(1) Yang, W.; Gan, L.; Li, H.; Zhai, T. Two-Dimensional Layered Nanomaterials for Gas-Sensing Applications. *Inorg. Chem. Front.* **2016**, *3* (4), 433–451. https://doi.org/10.1039/C5QI00251F.

(2) Sarkar, D.; Liu, W.; Xie, X.; Anselmo, A. C.; Mitragotri, S.; Banerjee, K. MoS_2 Field-Effect Transistor for Next-Generation Label-Free Biosensors. *ACS Nano* **2014**, *8* (4), 3992–4003. https://doi.org/10.1021/nn5009148.

(3) Li, H.; Yin, Z.; He, Q.; Li, H.; Huang, X.; Lu, G.; Fam, D. W. H.; Tok, A. I. Y.; Zhang, Q.; Zhang, H. Fabrication of Single- and Multilayer MoS_2 Film-Based Field-Effect Transistors for Sensing NO at Room Temperature. *Small* **2012**, *8* (1), 63–67. https://doi.org/10.1002/smll.201101016.

(4) Yang, S.; Jiang, C.; Wei, S. Gas Sensing in 2D Materials. *Appl. Phys. Rev.* **2017**, *4* (2), 021304. https://doi.org/10.1063/1.4983310.

(5) Perkins, F. K.; Friedman, A. L.; Cobas, E.; Campbell, P. M.; Jernigan, G. G.; Jonker, B. T. Chemical Vapor Sensing with Monolayer MoS_2. *Nano Lett.* **2013**, *13* (2), 668–673. https://doi.org/10.1021/nl3043079.

(6) Bergeron, H.; Sangwan, V. K.; McMorrow, J. J.; Campbell, G. P.; Balla, I.; Liu, X.; Bedzyk, M. J.; Marks, T. J.; Hersam, M. C. Chemical Vapor Deposition of Monolayer MoS_2 Directly on Ultrathin Al_2O_3 for Low-Power Electronics. *Appl. Phys. Lett.* **2017**, *110* (5), 053101. https://doi.org/10.1063/1.4975064.

(7) Cho, B.; Kim, A. R.; Park, Y.; Yoon, J.; Lee, Y.-J.; Lee, S.; Yoo, T. J.; Kang, C. G.; Lee, B. H.; Ko, H. C.; et al. Bifunctional Sensing Characteristics of Chemical Vapor Deposition Synthesized

Atomic-Layered MoS_2. *ACS Appl. Mater. Interfaces* **2015**, *7* (4), 2952–2959. https://doi.org/10.1021/am508535x.

(8) Xu, S.; Sun, F.; Yang, S.; Pan, Z.; Long, J.; Gu, F. Fabrication of SnO2-Reduced Graphite Oxide Monolayer-Ordered Porous Film Gas Sensor with Tunable Sensitivity through Ultra-Violet Light Irradiation. *Sci. Rep.* **2015**, *5* (1), 8939. https://doi.org/10.1038/srep08939.

(9) Kuru, C.; Choi, C.; Kargar, A.; Choi, D.; Kim, Y. J.; Liu, C. H.; Yavuz, S.; Jin, S. MoS_2 Nanosheet-Pd Nanoparticle Composite for Highly Sensitive Room Temperature Detection of Hydrogen. *Adv. Sci.* **2015**, *2* (4), 1500004. https://doi.org/10.1002/advs.201500004.

(10) Sarkar, D.; Xie, X.; Kang, J.; Zhang, H.; Liu, W.; Navarrete, J.; Moskovits, M.; Banerjee, K. Functionalization of Transition Metal Dichalcogenides with Metallic Nanoparticles: Implications for Doping and Gas-Sensing. *Nano Lett.* **2015**, *15* (5), 2852–2862. https://doi.org/10.1021/nl504454u.

(11) Zhao, P. X.; Tang, Y.; Mao, J.; Chen, Y. X.; Song, H.; Wang, J. W.; Song, Y.; Liang, Y. Q.; Zhang, X. M. One-Dimensional MoS_2-Decorated TiO_2 Nanotube Gas Sensors for Efficient Alcohol Sensing. *J. Alloys Compd.* **2016**, *674*, 252–258. https://doi.org/10.1016/j.jallcom.2016.03.029.

(12) Cui, S.; Wen, Z.; Huang, X.; Chang, J.; Chen, J. Stabilizing MoS_2 Nanosheets through SnO_2 Nanocrystal Decoration for High-Performance Gas Sensing in Air. *Small* **2015**, *11* (19), 2305–2313. https://doi.org/10.1002/smll.201402923.

(13) Long, H.; Harley-Trochimczyk, A.; Pham, T.; Tang, Z.; Shi, T.; Zettl, A.; Carraro, C.; Worsley, M. A.; Maboudian, R. High Surface Area MoS_2/Graphene Hybrid Aerogel for Ultrasensitive NO_2 Detection. *Adv. Funct. Mater.* **2016**, *26* (28), 5158–5165. https://doi.org/10.1002/adfm.201601562.

(14) Xin, X.; Zhang, Y.; Guan, X.; Cao, J.; Li, W.; Long, X.; Tan, X. Enhanced Performances of PbS Quantum-Dots-Modified MoS_2 Composite for NO_2 Detection at Room Temperature. *ACS Appl. Mater. Interfaces* **2019**, *11* (9), 9438–9447. https://doi.org/10.1021/acsami.8b20984.

(15) Han, Y.; Ma, Y.; Liu, Y.; Xu, S.; Chen, X.; Zeng, M.; Hu, N.; Su, Y.; Zhou, Z.; Yang, Z. Construction of MoS_2/SnO_2 Heterostructures for Sensitive NO2 Detection at Room Temperature. *Appl. Surf. Sci.* **2019**, *493*, 613–619. https://doi.org/10.1016/j.apsusc.2019.07.052.

(16) Hong, H. S.; Phuong, N. H.; Huong, N. T.; Nam, N. H.; Hue, N. T. Highly Sensitive and Low Detection Limit of Resistive NO_2 Gas Sensor Based on a MoS_2/Graphene Two-Dimensional Heterostructures. *Appl. Surf. Sci.* **2019**, *492*, 449–454. https://doi.org/10.1016/j.apsusc.2019.06.230.

(17) Sharma, S.; Kumar, A.; Kaur, D. Room Temperature Ammonia Gas Sensing Properties of MoS_2 Nanostructured Thin Film; 2018; p 030261. https://doi.org/10.1063/1.5032596.

(18) Kumar, R.; Goel, N.; Kumar, M. High Performance NO_2 Sensor Using MoS_2 Nanowires Network. *Appl. Phys. Lett.* **2018**, *112* (5), 053502. https://doi.org/10.1063/1.5019296.

(19) Cho, S.-Y.; Kim, S. J.; Lee, Y.; Kim, J.-S.; Jung, W.-B.; Yoo, H.-W.; Kim, J.; Jung, H.-T. Highly Enhanced Gas Adsorption Properties in Vertically Aligned MoS_2 Layers. *ACS Nano* **2015**, *9* (9), 9314–9321. https://doi.org/10.1021/acsnano.5b04504.

(20) Cho, B.; Hahm, M. G.; Choi, M.; Yoon, J.; Kim, A. R.; Lee, Y.-J.; Park, S.-G.; Kwon, J.-D.; Kim, C. S.; Song, M.; et al. Charge-Transfer-Based Gas Sensing Using Atomic-Layer MoS_2. *Sci. Rep.* **2015**, *5* (1), 8052. https://doi.org/10.1038/srep08052.

(21) Yuan, W.; Liu, A.; Huang, L.; Li, C.; Shi, G. High-Performance NO_2 Sensors Based on Chemically

Modified Graphene. *Adv. Mater.* **2013**, *25* (5), 766–771. https://doi.org/10.1002/adma.201203172.

(22) Yue, Q.; Shao, Z.; Chang, S.; Li, J. Adsorption of Gas Molecules on Monolayer MoS_2 and Effect of Applied Electric Field. *Nanoscale Res. Lett.* **2013**, *8* (1), 425. https://doi.org/10.1186/1556-276X-8-425.

(23) Baek, J.; Yin, D.; Liu, N.; Omkaram, I.; Jung, C.; Im, H.; Hong, S.; Kim, S. M.; Hong, Y. K.; Hur, J.; et al. A Highly Sensitive Chemical Gas Detecting Transistor Based on Highly Crystalline CVD-Grown $MoSe_2$ Films. *Nano Res.* **2017**, *10* (6), 1861–1871. https://doi.org/10.1007/s12274-016-1291-7.

(24) Park, H.; Han, G.; Lee, S. W.; Lee, H.; Jeong, S. H.; Naqi, M.; AlMutairi, A.; Kim, Y. J.; Lee, J.; Kim, W.; et al. Label-Free and Recalibrated Multilayer MoS_2 Biosensor for Point-of-Care Diagnostics. *ACS Appl. Mater. Interfaces* **2017**, *9* (50), 43490–43497. https://doi.org/10.1021/acsami.7b14479.

(25) Yoon, Y.; Ganapathi, K.; Salahuddin, S. How Good Can Monolayer MoS_2 Transistors Be? *Nano Lett.* **2011**, *11* (9), 3768–3773. https://doi.org/10.1021/nl2018178.

(26) Liu, Z.; Ma, L.; Junaid, A. S. M. NO and NO_2 Adsorption on Al_2O_3 and Ga Modified Al_2O_3 Surfaces: A Density Functional Theory Study. *J. Phys. Chem. C* **2010**, *114* (10), 4445–4450. https://doi.org/10.1021/jp907925w.

(27) Fan, Z.; Lu, J. G. Gate-Refreshable Nanowire Chemical Sensors. *Appl. Phys. Lett.* **2005**, *86* (12), 123510. https://doi.org/10.1063/1.1883715.

FIGURES AND CAPTIONS

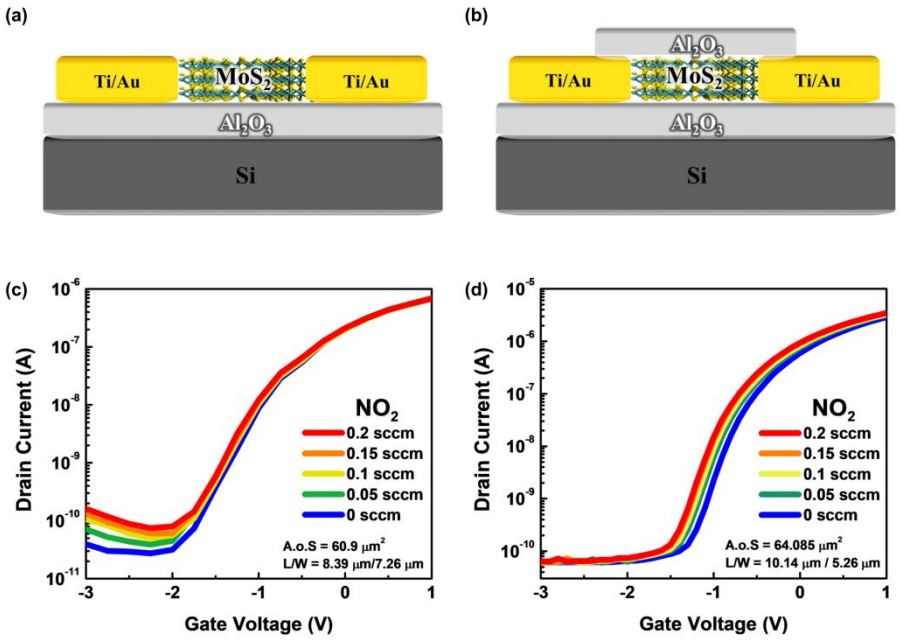

Figure 1. Schematic images of (a) a non-passivated MoS_2 TFT and (b) a passivated MoS_2 TFT. I_{DS}–V_{GS} curves showing the response of (c) the non-passivated MoS_2 TFT and (d) the passivated MoS_2 TFT to NO_2 gas.

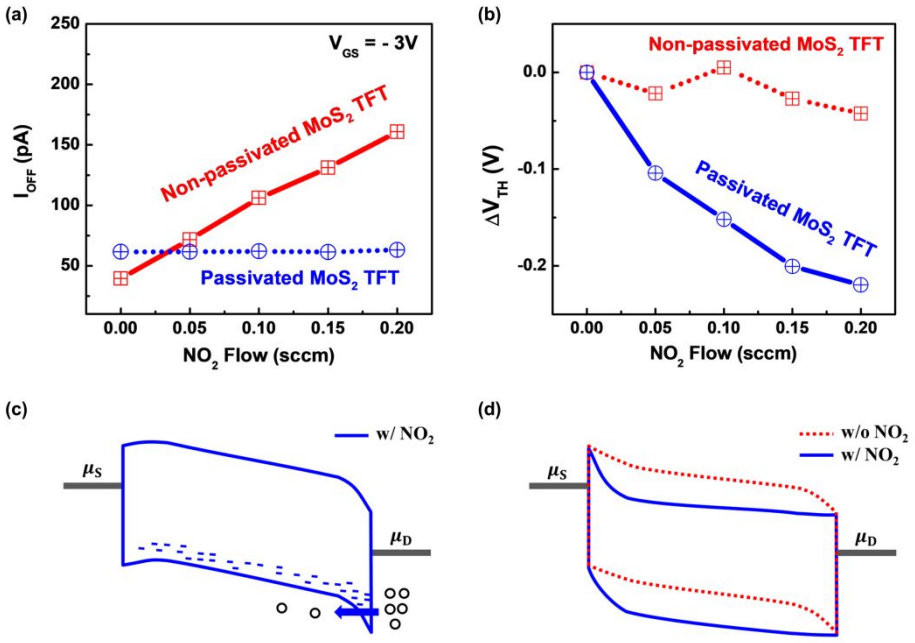

Figure 2. Device structure-dependent response of MoS_2 TFTs to NO_2 gas. (a) OFF-state current vs. NO_2 flow. (b) ΔV_{TH} vs. NO_2 flow. Energy band diagrams of (c) the non-passivated MoS_2 TFT and (d) the passivated MoS_2 TFT in the presence of NO_2 gas.

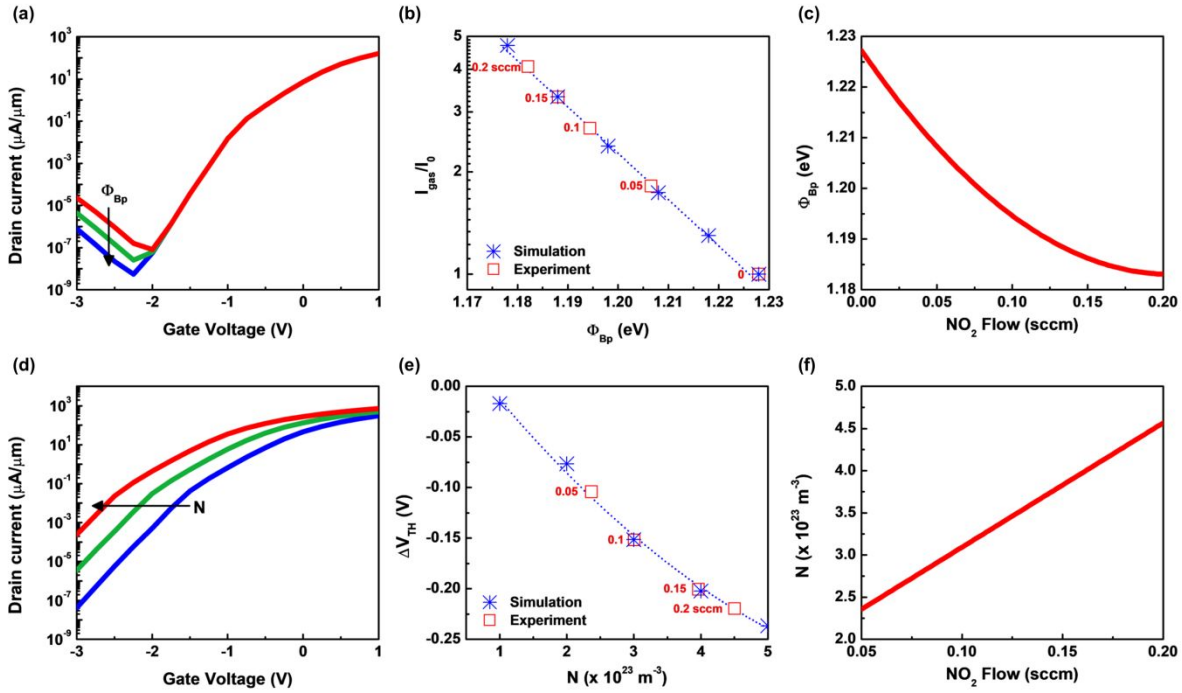

Figure 3. (a) Simulated I_{DS}–V_{GS} for the non-passivated device with the effective Schottky barrier height for holes (Φ_{Bp}) of 1.13, 1.18 and 1.23 eV (red, green and blue, respectively). (b) I_{gas}/I_0 vs. Φ_{Bp} calculated at V_{GS} = -3V from the simulation results (blue asterisks) and the experimental results (red squares). The dotted blue line is the fitting to the simulation data. (c) The relation between Φ_{Bp} and NO_2 gas flow, showing decrease in Φ_{Bp} in response to the increase of NO_2 flow. (d) Simulated I_{DS}–V_{GS} of the passivated device with the positive charge density of N = 0 (blue), 2 × 10^{23} m^{-3} (green), and 4 × 10^{23} m^{-3} (red) on the secondary gate dielectric. (e) V_{TH} shift (ΔV_{TH}) as a function of the charge density, N. The simulated results are shown in blue asterisks and experimental data in red squares. The dotted blue line is the fitting to the simulation data. (f) The relation between ΔV_{TH} and NO_2 gas flow.

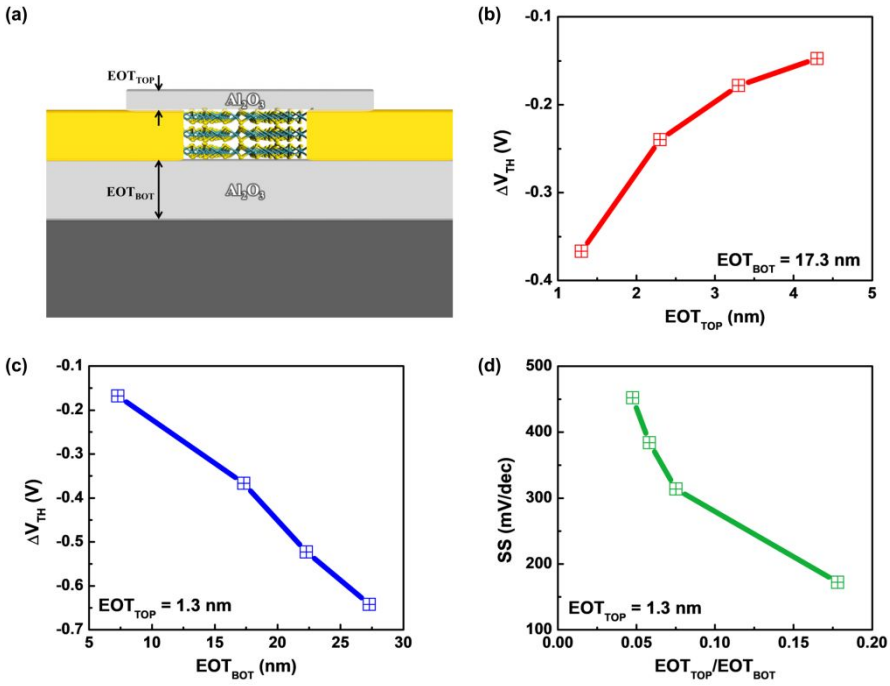

Figure 4. (a) Cross-section of the passivated device showing the parameters EOT_{TOP} and EOT_{BOT} varied for optimization. (b) ΔV_{TH} as a function of EOT_{TOP} (at a fixed EOT_{BOT} = 17.3 nm). (c) Effect of EOT_{BOT} variation on the V_{TH} shift (at a fixed EOT_{TOP} = 1.3 nm). (d) Subthreshold swing (SS) plotted as a function of EOT_{TOP}/EOT_{BOT} for the case shown in Figure 4c.

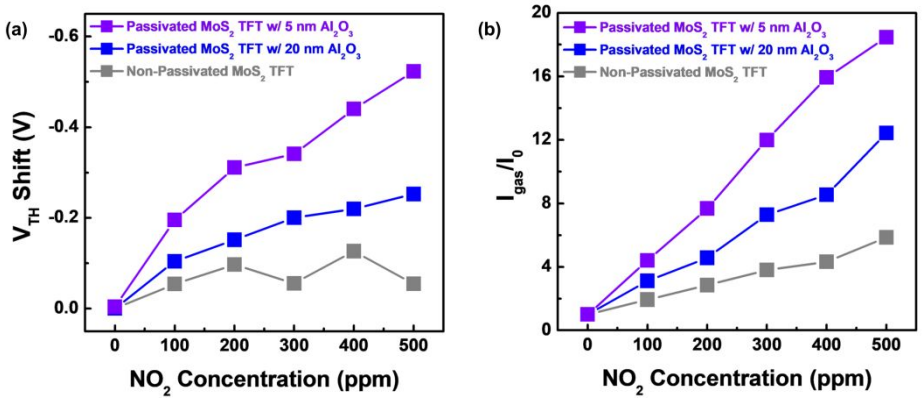

Figure 5. Responses to NO_2 gas with different device structures. (a) V_{TH} shift and (b) I_{gas}/I_0 as a function of NO_2 concentration.

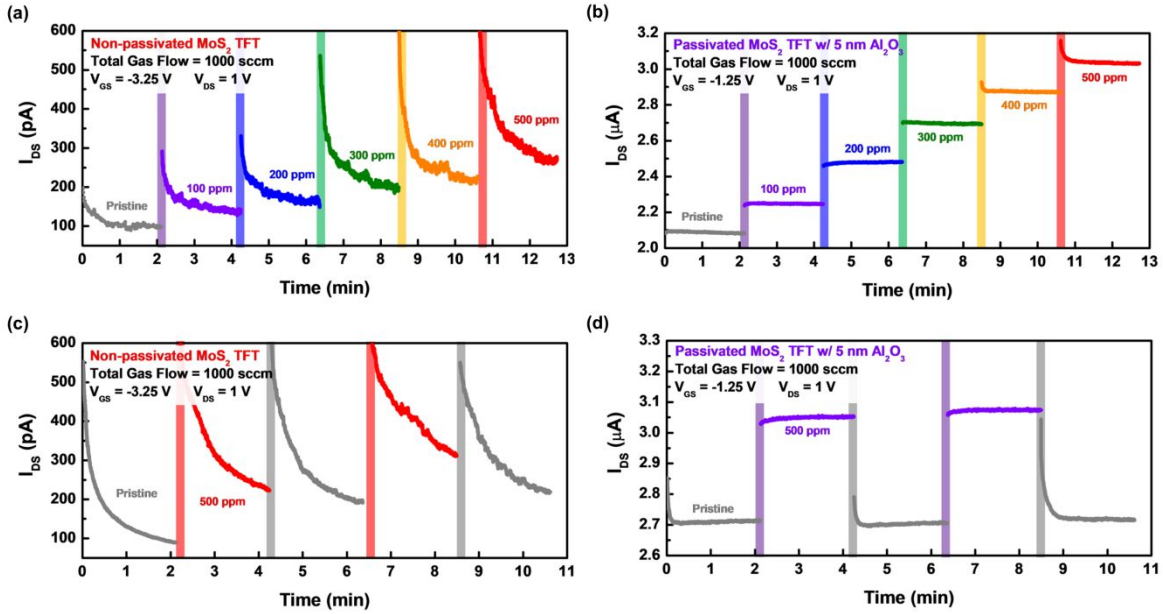

Figure 6. Time-resolved current responses of (a) non-passivated MoS_2 TFT and (b) passivated MoS_2 TFT with 5 nm-thick Al_2O_3 with different NO_2 gas concentration (vertical color lines depict 10 min of exposure time; not scaled). Time-resolved ON-OFF switching responses of (c) non-passivated MoS_2 TFT and (d) passivated MoS_2 TFT with 5 nm-thick Al_2O_3 at a NO_2 gas concentration of 500 ppm (vertical color lines depict 10 min of exposure time; gray lines 1 min of NO_2 gas removal from MoS_2 TFTs by applying V_{GS} of 30 V; not scaled).

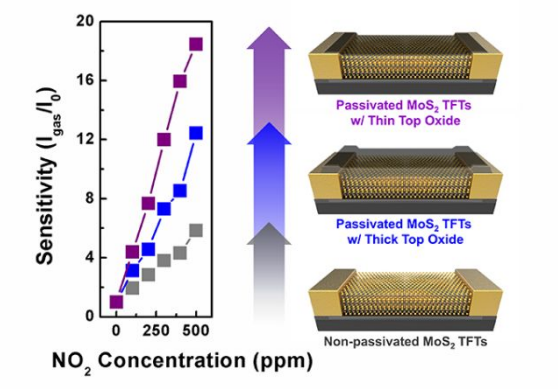
Sensitivity (I_{gas}/I_0)
20
16
12
8
4
0
0
250
500
NO_2 Concentration (ppm)
Passivated MoS_2 TFTs w/ Thin Top Oxide
Passivated MoS_2 TFTs w/ Thick Top Oxide
Non-passivated MoS_2 TFTs

For TOC only